Multi-$\mathcal{H}_\infty$ Controller Design and Illustration on an Overhead Crane

Keivan Zavari, Goele Pipeleers and Jan Swevers

***Abstract*— While reliable and efficient tools are widely available to solve (full-order) $\mathcal{H}_\infty$ control problems, formulating appropriate weighting functions constitutes the main obstacle to a good $\mathcal{H}_\infty$ controller design. In order to facilitate the weighting function design, we propose to break apart the classical $\mathcal{H}_\infty$ objective into various $\mathcal{H}_\infty$ design objectives and constraints, each relating to a particular closed-loop subsystem. The result is a versatile and intuitive control design approach, and the resulting control problem is solved using the Lyapunov shaping paradigm. The potential of our approach is demonstrated on an overhead crane setup.**

I. Introduction

The $\mathcal{H}_\infty$ control problem concerns the design of a stabilizing controller K that minimizes the $\mathcal{H}_\infty$ norm of the closed-loop system H:

$$\underset{K\in\mathcal{S}}{\text{minimize}} \quad \nu \tag{1a}$$

$$\text{subj. to} \quad \|H\|_\infty < \nu\,, \tag{1b}$$

where $\mathcal{S}$ denotes the set of internally stabilizing controllers. By the end of the 90's this problem was solved from a theoretical and mathematical viewpoint, at least for full-order controllers. Two alternative solution strategies, i.e. one based on Ricatti equations [1] and one based on linear matrix inequalities [2], [3], were developed and translated into reliable software, such as the function `hinfsyn` of the Matlab® Robust Control Toolbox™. In spite of its theoretical maturity, $\mathcal{H}_\infty$ control is generally not acknowledged as an easy and intuitive control design strategy. This is primarily due to the fact that a closed-loop $\mathcal{H}_\infty$ norm *an sich* has limited practical value and invokes the addition of weighting functions. Designing appropriate weighing functions is often an iterative and cumbersome process, where the laborious iterations in this design primarily follow from the fact that all the control objectives and constraints, generally relating to particular closed-loop *subsystems*, need to be merged into one artificial objective (1a): the $\mathcal{H}_\infty$ norm of the *overall* closed-loop system.

In order to facilitate the weighting function design, we propose to solve the controller design as a multi-objective control problem comprising multiple $\mathcal{H}_\infty$ norms on closed-loop subsystems. This results in a more intuitive control problem formulation compared to (1) as it allows distinguishing between design objectives and constraints, and imposing them on selected closed-loop subsystems. However, contrary to (1), no exact convex reformulation of the proposed controller design problem currently exists. We therefore resort to the Lyapunov shaping paradigm [4], a convex, yet conservative, solution strategy for general multi-objective control problems. Another solution strategy can be using the less conservative G-shaping paradigm in [5]. However, the paper's major contribution is in formulating the problem and showing that it simplifies the weighting function design; more than in solving the problem. The numerical results presented in Section III support the value of our design strategy in spite of the conservatism introduced by the Lyapunov shaping paradigm.

The contents of this paper is laid out as follows: Section II describes the control problem formulation together with the numerical solution strategy, while Section III numerically and experimentally demonstrates its potential on an overhead crane example. Section IV concludes the paper.

Notation The set of integers is indicated by $\mathbf{N}$, and $\mathbf{S}_n$ is the set of real symmetric $n \times n$ matrices. For a matrix $X \in \mathbf{S}_n$, the inequalities $X \prec 0$ and $X \succ 0$ mean X is negative definite, respectively positive definite.

II. Multi-$\mathcal{H}_\infty$ Controller Design

Section II-A presents the control problem formulation, while Section II-B describes the numerical solution of the resulting multi-objective control problem.

A. Problem Formulation

We consider a multi-objective control problem involving various $\mathcal{H}_\infty$ specifications on selected closed-loop subsystems. The problem is formulated in the general control configuration as depicted in Figure 1. The system P denotes the generalized plant and includes the weighting functions, K is the controller to be designed and H denotes the closed-loop system. The signals u and y respectively correspond to the control signal and the measured output, while the $\mathcal{H}_\infty$ design specifications are formulated by means of the exogenous input w and the regulated output z. The considered $\mathcal{H}_\infty$-norms are labelled by the index $i \in \mathcal{I} \subset \mathbf{N}$, and the ith norm is imposed on closed-loop subsystem H_i of the following form:

$$H_i = L_i H R_i\,, \tag{2}$$

where the matrices L_i, R_i select the appropriate input/output channels. The set $\mathcal{I} = \mathcal{I}_\text{c} \cup \mathcal{I}_\text{o}$, where $\mathcal{I}_\text{c}$ groups the indices relating to design constraints, while $\mathcal{I}_\text{o}$ relates to the design objectives. The order of P is denoted by n, and only the full-order controller design is considered. That is: the controller K is parametrized as a dynamical system of the same order n as the generalized plant P. The controller parameters are

Keivan Zavari, Goele Pipeleers and Jan Swevers are with the Department of Mechanical Engineering, Katholieke Universiteit Leuven, Celestijnenlaan 300B, B-3001 Heverlee, Belgium, keivan.zavari@mech.kuleuven.be.

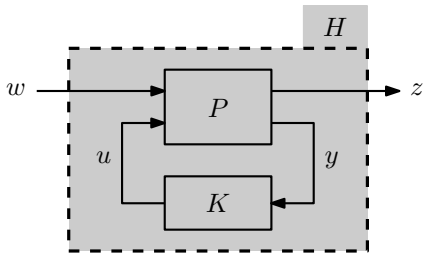

Fig. 1. General control configuration for the multi-$\mathcal{H}_\infty$ controller design. The $\mathcal{H}_\infty$ norms are imposed on subsystems $H_i = L_i H R_i$ for $i \in \mathcal{I}$.

computed as the optimal solution of the following problem:

$$\begin{aligned} \underset{K\in\mathcal{S}_n,\gamma_i}{\text{minimize}} \quad & \sum_{i\in\mathcal{I}_\text{o}} \alpha_i\gamma_i && && \text{(3a)}\\ \text{subj. to} \quad & \|H_i\|_\infty < \gamma_i\,, && \forall i\in\mathcal{I} && \text{(3b)}\\ & \gamma_i = 1\,, && \forall i\in\mathcal{I}_\text{c}\,, && \text{(3c)} \end{aligned}$$

where we added the subscript n to $\mathcal{S}$ to emphasize the controller order. In the sequel, the state-space model of the closed-loop system H is indicated as follows:

$$H : \begin{cases} \delta x &= Ax + Bw \\ z &= Cx + Dw \end{cases},$$

where δ denotes the one-shift-advance operator for the discrete-time case or the differentiator for continuous time. The dependency of A, B, C, D on the controller K is not mentioned explicitly for reasons of conciseness. The matrices B_i, C_i and D_i are defined as follows:

$$B_i = BR_i\,, \quad C_i = L_iC\,, \quad D_i = L_iDR_i\,.$$

B. Numerical Solution

The synthesis problem (3) is a multi-objective control problem and to date, no exact convex reformulation of such problems exists. Here, the problem is solved using the Lyapunov shaping paradigm [4], a convex, yet conservative solution approach for general multi-objective control problems. For a discrete-time control problem, this approach relies on the following, conservative, reformulation of (3):

$$\begin{aligned} \text{minimize} \quad & \sum_{i\in\mathcal{I}_\text{o}} \alpha_i\gamma_i^2 && && \text{(4a)}\\ \text{subj. to} \quad & Q \succ 0 && && \text{(4b)}\\ & \begin{bmatrix} A^TQA - Q & A^TQB_i & C_i^T \\ B_i^TQA & B_i^TQB_i - \gamma_i I & D_i^T \\ C_i & D_i & -\gamma_i I \end{bmatrix} \prec 0\,,\ \forall i\in\mathcal{I} && && \text{(4c)}\\ & \gamma_i = 1\,,\ \ \forall i\in\mathcal{I}_\text{c}\,, && && \text{(4d)} \end{aligned}$$

where the optimization variables are the Lyapunov matrix $Q \in \mathcal{S}_{2n}$, $K \in \mathcal{S}_n$ and γ_i. The corresponding reformulation for the continuous-time case can be found in [4]. The conservatism of the Lyapunov shaping paradigm stems from the fact that the same Lyapunov matrix Q is used in all the matrix inequalities. Problem (4) is transformed into a convex problem by means of the nonlinear change of controller variables presented in [4], [6].

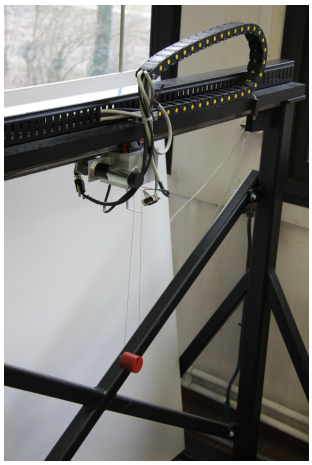

Fig. 2. The overhead crane test setup.

III. Numerical and Experimental Illustration

To illustrate the potential of the proposed controller design strategy, it is applied to investigate the trade-off between load tracking and disturbance rejection in the control of an overhead crane shown in Figure 2. Section III-A describes the model of the overhead crane, while Section III-B formulates the corresponding control problem. Section III-C presents the corresponding trade-off curve between load tracking and disturbance rejection, and Section III-D experimentally evaluates the obtained controllers.

A. System Model

The overhead crane system, schematically outlined in Figure 3, consists of a cart to which a load is attached by a rope. The rope has a fixed length $\ell = 0.45$ m and the cart position, load position and swing angle are indicated by x_c, x_L and θ, respectively. A linear idealized model of the overhead crane can be described as the following.

We assume that the cart is perfectly velocity controlled, such that $\dot{x}_c$ equals the external control input u:

$$\frac{x_c}{u} = \frac{1}{s}\,. \tag{5a}$$

In addition, the swing angle θ is assumed to be small such that the swing angle dynamics may by approximated to be linear time invariant:

$$\frac{\theta}{x_c} = \frac{-s^2}{s^2\ell + g}\,, \tag{5b}$$

and the load position $x_L = x_c + \ell\theta$. The corresponding undamped natural eigenfrequency equals $f_n = 0.74$ Hz. Both x_c and θ are measured by an encoder.

The overhead crane is identified and controlled as a discrete system with sampling frequency of 60 Hz using a dSpace CP1103 controller board in combination with Matlab Simulink® and ControlDesk®. This system is controlled

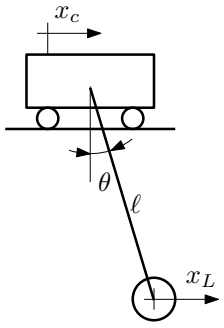

Fig. 3. Schematic outline of the overhead crane.

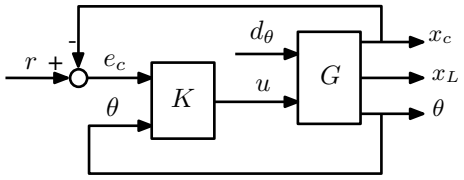

Fig. 4. Control configuration used for the overhead crane.

according to the configuration outlined in Figure 4. The system G represents the overhead crane and is governed by (5). Input r is the reference command and the disturbance input d_θ imposes swing angel disturbance such that the system response to an impulse in d_θ corresponds to the autonomous response from an initial swing angle $\theta_0 \neq 0$ rad.

B. Control Problem Formulation

The primal goal of the controller K is to make the load follow the reference command r. To this end, all measured signals are fed back to the controller:

$$y = \begin{bmatrix} r - x_c \\ \theta \end{bmatrix} = \begin{bmatrix} e_c \\ \theta \end{bmatrix} .$$

Superior load tracking requires a controller that does not excite the system's resonance and hence, has an anti-resonance at the eigenfrequency f_n. However, such a controller cannot compensate load swinging due to an initial angle deviation, as this compensation requires an harmonic control signal with frequency f_n. Consequently, load tracking and angle disturbance rejection are conflicting performance specifications in the controller design. We will investigate this trade-off with the help of the control strategy proposed in Section II. To this end, both specifications are quantified in terms of a weighted closed-loop $\mathcal{H}_\infty$ norm. Load tracking is quantified by $\gamma_e = \|W_e H_{r,e_L}\|_\infty$ where H_{r,e_L} denotes the closed-loop transfer function from r to $e_L = r - x_L$, and $W_e = 0.5\pi/s$. This weight enforces H_{r,e_L} to be of system type 1, and minimizing γ_e corresponds to maximizing the bandwidth. Load tracking is quantified by $\gamma_d = \|H_{d\theta,\theta}\|_\infty$, such that minimizing γ_d corresponds to maximizing the damping of f_n in $H_{d\theta,\theta}$: the closed-loop transfer function from $d\theta$ to θ. As a third specification in the controller design problem, a constraint on the actuator effort is added: $\|W_u H_{r,u}\|_\infty < 1$, where $H_{r,u}$ denotes the closed-loop transfer function from r to u and $W_u = s/(10\pi)$ to bound the derivative of u, which equals the cart acceleration.

To conclude, analyzing the trade-off between load tracking and angle disturbance rejection under bounded actuator effort amounts to solving the following control problem for various values of α:

$$\begin{aligned} \underset{K \in \mathcal{S}_5, \gamma_e, \gamma_d}{\text{minimize}} \quad & \gamma_e + \alpha\gamma_d && \text{(6a)} \\ \text{subj. to} \quad & \|W_e H_{r,e_L}\|_\infty < \gamma_e && \text{(6b)} \\ & \|H_{d_\theta,\theta}\|_\infty < \gamma_d && \text{(6c)} \\ & \|W_u H_{r,u}\|_\infty < 1 && \text{(6d)} \end{aligned}$$

This problem is of the form (3), which is clarified by grouping all exogenous inputs and regulated outputs in w, respectively z:

$$w = \begin{bmatrix} r \\ d\theta \end{bmatrix} , \quad z = \begin{bmatrix} W_e e_L \\ \theta \\ W_u u \end{bmatrix} .$$

Let H denote the overall closed-loop transfer matrix, then all the transfer functions considered in (6) are of the form (2) for some matrices L and R. For instance,

$$W_e H_{r,e_L} = \underbrace{\begin{bmatrix} 1 & 0 & 0 \end{bmatrix}}_{L} H \underbrace{\begin{bmatrix} 1 \\ 0 \end{bmatrix}}_{R} .$$

Instead of explicitly labelling all control specifications by the index i, we continue with the notation used in (6).

The control problem is solved in discrete time. Prior to solving (6), the weighting functions are discretized at a sample frequency of 60 Hz using the zero-order-hold transformation.

C. Trade-off between γ_e and γ_d

To analyze the trade-off between load tracking and angle disturbance rejection, a trade-off curve between γ_e and γ_d is computed. This is done by solving (6) using MATLAB in combination with the SeDuMi solver [7], and the YALMIP interface [8] for different values of α and plotting the optimal γ_e and γ_d values as a function of each other. This result is shown in black-dashed line in Figure 5.

By increasing α, the trade-off curves are traced from left to right, yielding better angle disturbance rejection, lower γ_d value, at the cost of degraded load tracking, higher γ_e value. The left-most point corresponds to the solution of (6) with $\alpha = 0$. The corresponding optimal controller is indicated by K_1, and the optimal performance indices equal $(\gamma_{e,1}, \gamma_{d,1}) = (0.696, 6380)$. The right-most point on the curve is obtained by considering $\alpha = \infty$, or equivalently, by replacing the objective (6a) by γ_d. The corresponding controller is indicated by K_2 and its performance indices equal $(\gamma_{e,2}, \gamma_{d,2}) = (3.9, 1.99)$.

The steep left part of the trade-off curve indicates that starting from K_1, γ_d can be decreased significantly with only a small increase in γ_e. The shallow right part, on the other hand, means that a controller can achieve significantly better load tracking performance than K_2 while have only slightly

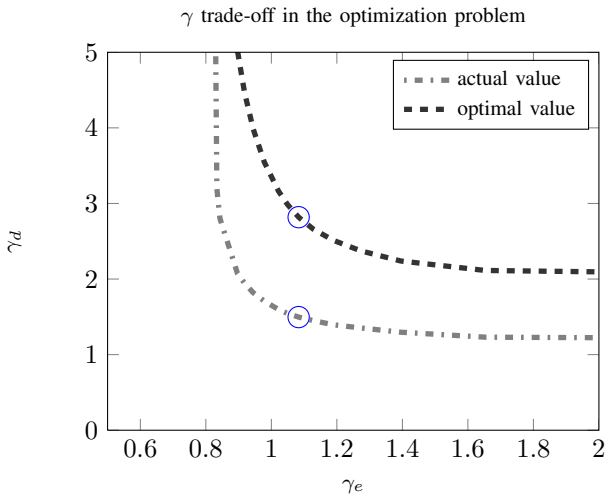

Fig. 5. Trade-off curves of tracking performance and disturbance rejection. The circled-blue point is the trade-off point which provides a good compromise between conflicting performances result.

TABLE I

COST FUNCTIONS OF THE MIXED-SENSITIVITY CONTROL PROBLEM.

	optimal γ	actual γ
$H_{r,e}$	1.083	1.083
$H_{r,u}$	1	0.7525
$H_{d_\theta,\theta}$	2.81	1.497

worse angle disturbance rejection. A good engineering choice would therefore be a controller that corresponds to a point on the trade-off curve with a moderate slope part, as for instance K_3, which is indicated by the blue circle in Figure 5.

To analyze the conservatism caused by the Lyapunov shaping paradigm used to solve the optimal control problem, the grey dashed-dotted line in Figure 5 shows the true values of $\gamma_e = \|W_e H_{r,e_L}\|_\infty$ and $\gamma_d = \|W_\theta H_{d\theta,\theta}\|_\infty$ achieved by the optimized controllers. Due to the conservatism, the optimized γ_e, γ_d values, obtained by solving (6) according to (4), provide only an upper bound to the true performance indices achieved by the optimized controller. Hence, in Figure 5 the black dashed line, indicating the optimized γ values, lies above the gray dashed-dotted line, indicating the actual γ values, and the distance between the curves is a measure for the conservatism of the Lyapunov shaping paradigm. Table I compares the optimized and actual γ values for controller K_3, and confirms that the optimized γ values provide only an upper bound to the actual closed-loop $\mathcal{H}_\infty$ norms.

D. Comparison of three controllers

In order to support the findings of the previous section, the controllers K_1, K_2 and K_3 are further compared and implemented on the overhead crane shown in Figure 2. Figure 6 compares closed-loop frequency response functions (FRFs) of H_{r,e_L}, $H_{r,u}$ and $H_{d\theta,\theta}$, while Figures 7 and 8 show their time-domain responses. Figure 7 shows the response to a step input of 10 cm in r and Figure 8 depicts an initial angel deviation of the load on the experimental test setup. By the construction of d_θ, the impulse responses from d_θ correspond to the autonomous responses from an initial swing angle deviation and in practice this is performed by manually applying an impulse disturbance to the load. Because it is not possible to manually apply the same disturbance to the angel at different experiments, the amplitudes are not the same value in Figure 8. In this case the shape of the response and settling time matter more.

The results for K_1, which yields the best load tracking, are shown in dashed-red. The dashed-dotted green lines correspond to K_2, which yields the best disturbance rejection, while the solid blue lines relate to K_3, which yields a good trade-off between load tracking and angle disturbance rejection.

Figure 6 confirms that K_1 yields the highest bandwidth for H_{r,e_L}. To achieve this superior load tracking performance K_1 must not excite the system's resonance, due to which it cannot counteract the swinging initiated by an initial angle deviation. Consequently, in the FRF of $H_{d_\theta,\theta}$ the system's undamped resonance at $f_n = 0.74$ Hz prevails. Figures 7 and 8 confirm the superior load tracking and poor disturbance rejection performance of K_1.

The controller K_2 yields superior disturbance rejection at the cost of very poor load tracking, is confirmed by Frequency- and time-domain responses. Controller K_3, on the other hand, yields a good compromise between the two performance aspects. Compared to K_1 it yields a slightly lower bandwidth in H_{r,e_L}, while providing much more damping to the resonance in $H_{d_\theta,\theta}$. Compared to K_2, K_3 gives a slightly higher $\|H_{d_\theta,\theta}\|_\infty$, while providing a significantly higher bandwidth in H_{r,e_L}. Figures 7 and 8 support these findings.

IV. CONCLUSION

This paper proposes to break apart the classical $\mathcal{H}_\infty$ control problem into $\mathcal{H}_\infty$ objectives and constraints on selected closed-loop subsystems. This results in a versatile and intuitive control design approach and facilitates the weighting function design for the various $\mathcal{H}_\infty$ specifications. The resulting multi-objective control problem is solved using the Lyapunov shaping paradigm. To illustrate proposed design approach it is applied to an overhead crane example to analyze the trade-off between angle disturbance rejection and load tracking. These results reveal the value of our approach despite its conservatism.

V. ACKNOWLEDGEMENT

Goele Pipeleers is a Postdoctoral Fellow of the Research Foundation Flanders (FWO Vlaanderen). This work benefits from K.U.Leuven BOF PFV/10/002 Center-of-Excellence Optimization in Engineering (OPTEC), the Belgian Programme on Interuniversity Attraction Poles, initiated by the Belgian Federal Science Policy Office (DYSCO), research projects G.0377.09 and G.0002.11 of the Research Foundation Flanders (FWO Vlaanderen), FP7- EMBOCON (ICT-248940), and K.U.Leuvens Concerted Research Action

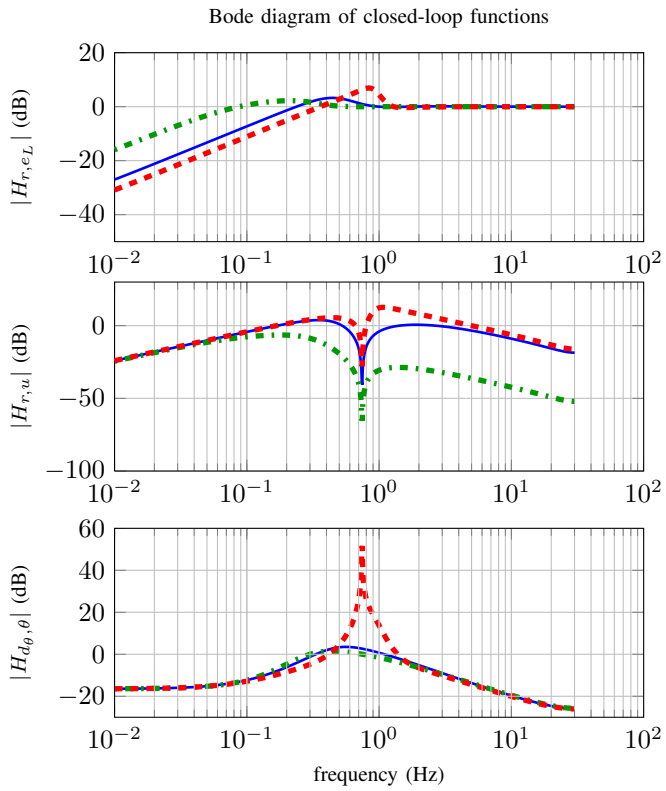

Fig. 6. Closed-loop Bode diagrams using the controller K_1 (dashed-red), K_2 (dash-dotted-green) and K_3 (solid-blue).

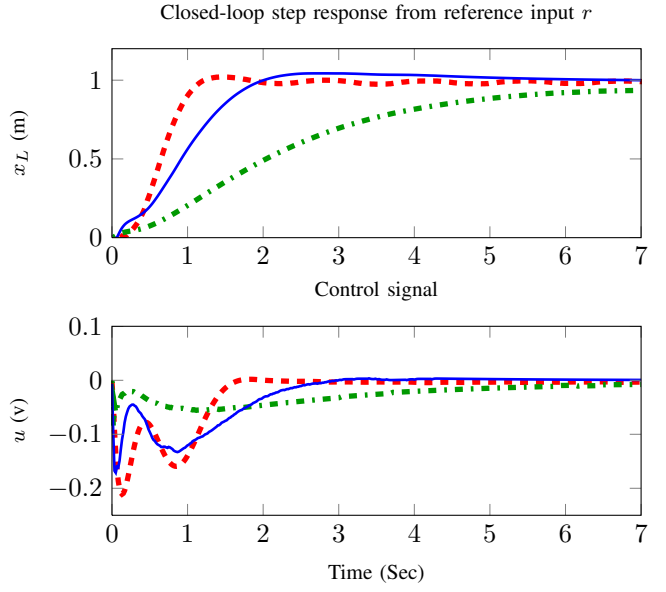

Fig. 7. Closed-loop reference step response (top figure) and corresponding control signal (bottom figure) using controller K_1 (dashed-red), K_2 (dash-dotted-green) and K_3 (solid-blue).

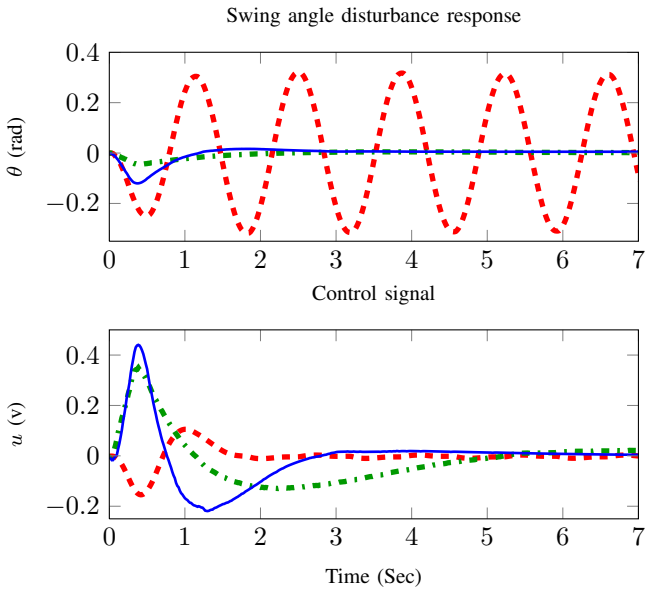

Fig. 8. Swing angle disturbance response (top figure) and corresponding control signal (bottom figure) using controller K_1 (dashed-red), K_2 (dash-dotted-green) and K_3 (solid-blue).

GOA/10/11 Global real-time optimal control of autonomous robots and mechatronic systems.

REFERENCES

[1] K. Glover and J. C. Doyle. State-space formulae for all stabilizing controllers that satisfy an $\mathcal{H}_\infty$-norm bound and relations to risk sensitivity. *Systems & Control Problems*, 11:167–172, 1988.

[2] T. Iwasaki and R. E. Skelton. All controllers for the general $\mathcal{H}_\infty$ control problem: LMI existence conditions and state space formulas. *Automatica*, 30(8):1307–1317, 1994.

[3] P. Gahinet and P. Apkarian. A linear matrix inequality approach to $\mathcal{H}_\infty$ control. *International Journal of Robust and Nonlinear Control*, 4:421–448, 1994.

[4] C. Scherer, P. Gahinet, and M. Chilali. Multiobjective output-feedback control via LMI optimization. *IEEE Transactions on Automatic Control*, 42(7):896–911, 1997.

[5] M. C. de Oliveira, J. C. Geromel, and J. Bernussou. Extended $\mathcal{H}_2$ and $\mathcal{H}_\infty$ norm characterizations and controller parametrizations for discrete-time systems. *Int. J. Control*, 75(9):666–679, 2002.

[6] I. Masubuchi, A. Ohara, and N. Suda. A linear matrix inequality approach to $\mathcal{H}_\infty$ control. *LMI-based controller synthesis: A unified formulation and solution*, 8(8):669–686, 1998.

[7] J. F. Sturm, "Using SeDuMi 1.02, a Matlab toolbox for optimization over symmetric cones," *Optimization Methods and Software*, vol. 11, pp. 625–653, 1999.

[8] J. Löfberg, "Yalmip : A toolbox for modeling and optimization in MATLAB," in *Proceedings of the CACSD Conference*, Taipei, Taiwan, 2004. [Online]. Available: `http://users.isy.liu.se/johanl/yalmip`